Discontinuous cellular automaton method for crack growth analysis without remeshing

Fei Yan *, Xia-Ting Feng, Peng-Zhi Pan, Shao-Jun Li

State Key Laboratory of Geomechanics and Geotechnical Engineering, Institute of Rock and Soil Mechanics, Chinese Academy of Science, Wuhan 430071, China

ARTICLE INFO

ABSTRACT

A numerical technical of discontinuous cellular automaton method for crack growth analysis without remeshing is developed. In this method, the level set method is employed to track the crack location and its growth path, where the level set functions and calculation grids are independent, so no explicit meshing for crack surface and no remeshing for crack growth are needed. Then, the discontinuous enrichment shape functions which are enriched by the Heaviside function and the exact near-tip asymptotic field functions are constructed to model the discontinuity of cracks. Finally, a discontinuous cellular automaton theory is proposed, which are composed of cell, neighborhood and updating rules for discontinuous case. There is an advantage that the calculation is only applied on local cell, so no assembled stiffness matrix but only cell stiffness is needed, which can overcome the stiffness matrix assembling difficulty caused by unequal degrees of nodal freedom for different cells, and much easier to consider the local properties of cells. Besides, the present method requires much less computer memory than that of XFEM because of it local property.

Combined level set method, the discontinuous enrichment shape functions and discontinuous cellular automaton theory, the discontinuous cellular automaton method is proposed, which can conveniently achieve the analysis from continuity to discontinuity. Numerical examples are given to illustrate that the present method is effective, and can be further extended into practical engineering.

© 2013 Elsevier Inc. All rights reserved.

1. Introduction

Failures in engineering structure are usually caused by some defects, such as cracks, inclusion and interface and so on, and many failures result largely from the microcracks which grow beyond a safety limit. While the cracks in engineering structures are always exist during manufacturing and service, and exact solutions for most of complex cracks growth are not available, so crack growth simulation is a challenging and important problem in practical engineering.

Crack is a discontinuous structure, and its propagation leads to the expansion of some local areas of structure from continuous into discontinuous, which brings some difficulty for many numerical methods. Finite element method has been firstly used to calculate stress intensity factors [1,2]. But it requires the element edges to coincide with the crack surface, and remeshing is inevitable when the discontinuous surface changes. Later, boundary element method [3,4], boundary integral equation method [5] and boundary collocation method [6,7], in which the mesh is only enforced on the boundary, have

 * Corresponding author. Address: State Key Laboratory of Geomechanics and Geotechnical Engineering, Institute of Rock and Soil Mechanics, Chinese Academy of Science, Xiaohongshan, Wu Chang, Wuhan 430071, China. Tel.: +86 27 87198805, mobile: +86 13477073381; fax: +86 27 87198413.
   E-mail address: fyan@whrsm.ac.cn (F. Yan).

been proposed to solve the fracture calculation, and those methods avoid a large part of remeshing because only the boundary is needed to be meshed.

Recently, the element-free Galerkin method [8–10] has been applied to fracture computation, and the essential feature of this methods is that they only require a set of nodes to construct the calculation model. Besides, meshless local Petrov–Galerkin method [11] and local boundary integral equation method [12] have been also applied to analyze growing crack problems. Additionally, numerical manifold method [13] has been also used to simulate the crack propagation, which is suitable to simulate continuous and discontinuous problems at the same frame, but its dual grid property causes some difficulty in some complex crack growth.

Recently, some methods in FE framework without remeshing have been developed. Using partition of unity [14], Belytschko and Black [15] first introduced a method for solving crack problem with FE framework. Later, Moes et al. [16] used the Heaviside function to describe the discontinuity across crack faces and developed crack tip enrichments. After that, a junction function concept has been introduced to solve multiple branched cracks [17], and extended finite element method (XFEM) has been developed in detail. Based on XFEM formulation, 2D and 3D crack growth analysis with or without contact friction have been developed by Sukumar et al. [18] and Dolbow et al. [19]. Besides, Xiao and Karihaloo [20] discussed the influence of quadrature rules on the accuracy of XFEM.

Incorporating the application of the analytical or numerical function into tradition FE approximation with the partition of unity, generalized finite element method [21–23] has been proposed to solve fracture mechanics, which can improve the local and global accuracy of numerical solutions. Those methods have been widely used to simulate crack growth problems, because the finite element mesh can be completely independent of the morphology of the model, and the crack surface and crack front are completely independent of the mesh, so no remeshing is needed in crack propagation simulation.

In order to track complex crack configurations, the level set method(LSM) was developed by Osher and Sethian [24], which was used for tracking the moving interface. Then the LSM was used to describe the topology changes of the interface. Later, Belytschko et al. [25] and Stolarska et al. [26] combined the LSM with the XFEM to study the growth of a fatigue crack and several frictionless contact problems. With the use of the LSM, the grid for XFEM is completely independent of the crack faces, so no remeshing is need for crack growth analysis.

It is known that the node freedoms are different for different nodes for XFEM, which brings some difficulty for global stiffness matrix assembling, besides, it takes a large amount of computer memory for this procedure. So the cellular automaton (CA) theory is used to overcome this defect. The cellular automaton (CA) theory was initially derived from the self-organization theory in biology. Shen et al. [27] developed elastic updating rules and applied it to solve the solid mechanical problem. Gurdal and Tatting [28] built a lattice model to solve the plane lattice deformation problem, additionally Hopman and Leamy [29], Leamy [30] developed an application of cellular automata modeling to elastodynamics problem and arbitrary two-dimensional geometries, and further Feng et al. [31] used the lattice CA model to simulate the failure process of heterogeneous rocks. There are two advantages of the application of CA model, one is the calculation only applied on local cell, so no assembled stiffness matrix but only cell stiffness is needed, which can overcome the stiffness matrix assembling difficulty caused by unequal degrees of nodal freedom for different cells, and much easier to consider the local property of node and element. Another is that it can be easily extended to the large-scale simulation for its easy implementation of the parallel algorithm. Besides, much less computer memory requirement is achieved because of it local property.

As the discontinuous numerical methods, DEM [32] and DDA [33] are widely used in soil and rock engineering. Those two methods are based block theory, which can simulate the moving, rotating, opening and clogging of rock blocks. When those methods are applied to simulate the crack growth, its growth path can only be along to the block boundary, and its fracture cannot extend into the blocks, but we do not know the direction of the propagation of crack before its growth. So those two methods are suitable for solving the known discontinuous structure problems, and can not accurately achieve the expansion from continuity to discontinuity.

In this work, discontinuous enrichment shape function, level set method and discontinuous cellular automaton theory are combined, and a numerical technical of discontinuous cellular automaton method is proposed, in which the calculation is only applied on local elements and nodes, and no assembled stiffness matrix is needed, so it is much easier to consider the local property of material and its interaction. Firstly, the level set method is employed to track the crack location and its growth path, in which the level set functions and calculation grid are independent, so no explicit meshing for crack surface and no remeshing for crack growth are needed. Then, the discontinuous enrichment shape functions which are enriched by the Heaviside function and the exact near-tip asymptotic field functions are constructed to model the discontinuity of cracks. Finally, a discontinuous cellular automaton theory is proposed, in which the calculation is only applied on local cell, so no assembled stiffness matrix but only cell stiffness is needed.

2. Continuous and discontinuous structure modeling

Crack is a strong discontinuous structure, and in the traditional finite element the crack surface should coincide with the element edge in order to model the strong discontinuous displacement and stress field. In this work, approximation of the discontinuous displacement field is based on a specially designed shape functions, in which the Heaviside function is used to simulate the discontinuity and the exact near-tip asymptotic field functions is employed to model the high gradient stress field near the crack tip.

2.1. Grid model

In present method, crack model and element grid are independent in the calculation, so some elements are penetrated by crack, and the crack tip can locate on any element of the model. In order to model the discontinuity of crack surface and the high gradient stress field around the crack tip, some nodes are needed to enrich by some special functions. Therefore, the classical finite elements can be divided into three groups, one is standard finite element, and another is penetrated element, which is penetrated by the crack, but crack tip is not located on, and the third one is crack tip element, on which crack tip is located. In order to improve the calculation accuracy, the nodes which are located at a limited distance from the crack tip are also chosen as the crack tip nodes, which can be seen in Fig. 1.

It can be seen in Fig. 1 that the node firstly belongs to set T, which is crack tip nodes set; then it is a part of nodes set P, the others are included in common nodes of standard finite element method.

2.2. Modeling method of strong discontinuous structure

According to partition of unity theory [14], a enriched shape function on a general point $\mathbf{x}$ within a finite element can be given as

$$\mathbf{u}^h(\mathbf{x}) = \sum_{j=1}^{n} N_j(\mathbf{x})\left(\mathbf{u}_j + \sum_{k=1}^{m} p_k(\mathbf{x})\mathbf{a}_{jk}\right) \tag{1}$$

In which $N_j(\mathbf{x})$ is the classical finite element shape function; $\mathbf{u}_j$ is the nodal displacements, which is the standard degree of freedom; and $p_k(\mathbf{x})$ is enriched function; $\mathbf{a}_{jk}$ is a vector of additional degree of nodal freedom for modeling strong discontinuity.

It is known to us that the displacements on the nodes of upper and bottom surface of crack are different, in order to model the strong discontinuity caused by the crack, the signed function is chosen as the Heaviside enrichment function, which is given as

$$H(\xi) = \text{sign}(\xi) = \begin{cases} 1 & \forall \xi > 0, \\ -1 & \forall \xi < 0. \end{cases} \tag{2}$$

In which ξ is the value of level set function, which will be given in the next section (in Fig. 2).

As we know, Eq. (1) is not an interpolation and the nodal parameter $\mathbf{u}_j$ is not the real displacement value on enriched node j. In order to satisfy interpolation at nodal points, and substitute Eq. (2) into Eq. (1), one can get [34]

$$\mathbf{u}^h(\mathbf{x}) = \sum_{j=1}^{n} N_j(\mathbf{x})\mathbf{u}_j + \underbrace{\sum_{k=1}^{m} N_k(\mathbf{x})(H(\xi) - H(\xi_k))\mathbf{a}_k}_{k \in P}. \tag{3}$$

In which n and m are the node numbers of element, P is the penetrated nodes set, which can be seen in Fig. 1. In this equation, the interpolation can be automatically guaranteed.
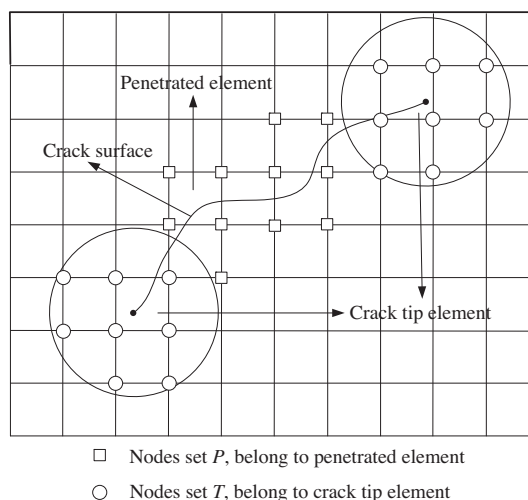

□　Nodes set P, belong to penetrated element

○　Nodes set T, belong to crack tip element
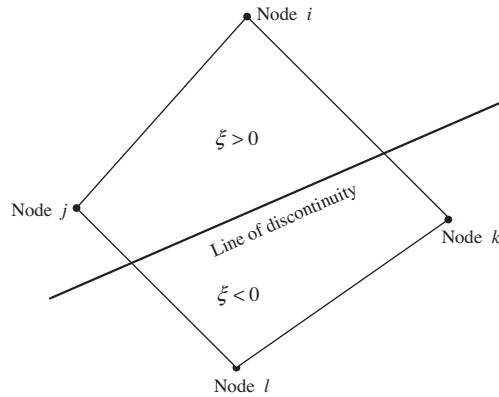
Fig. 1. Elements and nodes model.

Fig. 2. An element cut cross by a crack.

According to Eq. (3), the overall jump in the displacement field can be obtained, which is

$$\langle \mathbf{u}^h(\mathbf{x}) \rangle = \mathbf{u}^h(\mathbf{x}^+) - \mathbf{u}^h(\mathbf{x}^-) = \sum_{k=1}^{m} N_k(\mathbf{x})\mathbf{a}_k. \tag{4}$$

It can be seen that application of this jump function on a element can lead to a discontinuous field.

2.3. Modeling method of crack tip stress field

It is well known that a high gradient stress field exists around the crack tip. In order to get much higher accuracy, element refinement is needed around the crack tip in traditional finite element method. So as to accurately model the crack tip stress field without element refinement, shape functions enriched by the exact near-tip asymptotic field functions are applied.

The same as Eq. (3), one can get

$$\mathbf{u}^h(\mathbf{x}) = \sum_{j=1}^{n} N_j(\mathbf{x})\mathbf{u}_j + \underbrace{\sum_{k=1}^{m} N_k(\mathbf{x})(H(\xi) - H(\xi_k))\mathbf{a}_k}_{k \in P} + \underbrace{\sum_{i=1}^{t} N_i(\mathbf{x})\left(\sum_{l=1}^{nf} (F_l(\mathbf{x}) - F_l(\mathbf{x}_i))\mathbf{b}_i^l \right)}_{i \in T}, \tag{5}$$

where t is node number associated with crack tip, and T is crack tip nodes set, which can be seen in Fig. 1; nf is the number of the exact near-tip asymptotic field functions; $\mathbf{b}_i^l$ is a vector of additional degrees of nodal freedom for modeling crack tip stress field, and $F_l(\mathbf{x})$ is the exact near-tip asymptotic field functions, which can be given as [34]

$$\{F_l(x), l = 1 - 4\} = \left\{ \sqrt{r}\sin\left(\frac{\theta}{2}\right), \sqrt{r}\cos\left(\frac{\theta}{2}\right), \sqrt{r}\sin(\theta)\sin\left(\frac{\theta}{2}\right), \sqrt{r}\sin(\theta)\cos\left(\frac{\theta}{2}\right) \right\}. \tag{6}$$

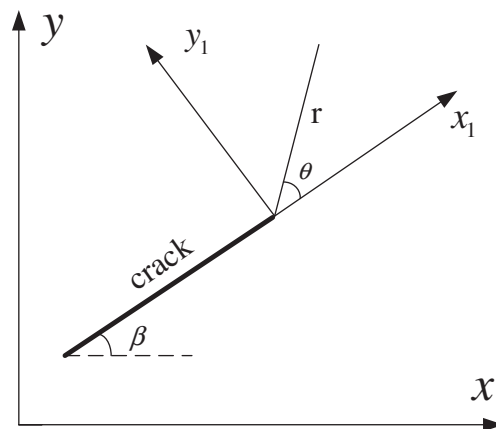In which r, θ can be seen in Fig. 3.

Fig. 3. Coordinate system of crack tip.

It can be seen that Eq. (5) satisfies the interpolation at nodal points, and the high gradient stress field around crack tip is modeled by the exact near-tip asymptotic field functions enriched shape functions, by which the calculation accuracy can be greatly improved around crack tip.

It can be seen from aforementioned theory that only classical finite element grid is needed, and the enrichment is only enforced on a small part of nodes, for example, the Heaviside function enrichment is only carried out on the nodes whose elements are penetrated by the crack, and the exact near-tip asymptotic field functions enrichment is only enforced on the nodes which are located at a limited distance from the crack tip.

3. Tracking crack growth paths

A powerful tool for tracking moving interface is the level set method, which is first introduced by Osher and Sethian [24], and the present method can benefit greatly by the level set method. The level set method is based on the idea of representing the moving interface as a level set curve of a higher-dimensional function $\varphi(\mathbf{x}, t)$.

3.1. Tracking crack surface

In this method, the level set method is used to track the growth crack. In the level set method, the moving interface of interest is represented as the zero level set function of $\varphi(\mathbf{x}, t)$. Then, the evolution for the moving interface can be expressed as an evolution of equation $\varphi(\mathbf{x}, t)$.

In general, a crack surface $\gamma(t) \subset R^2$ can be expressed as the level set curve of a function $\varphi(\mathbf{x}, t) = 0$ [26,35], which is shown in Fig. 4, and the expression is given as

$$\gamma(t) = \{\mathbf{x} \in R^2 : \varphi(\mathbf{x}, t) = 0\}. \tag{7}$$

Taken the Fig. 4 as the example, the level set function $\varphi(\mathbf{x}, t)$ would be the signed distance function, which is

$$\varphi(\mathbf{x}, t) = \xi(\mathbf{x}, t) = \min_{\mathbf{x}_\Gamma \in \Gamma(t)} \|\mathbf{x} - \mathbf{x}_\Gamma\| \cdot \text{sign}(\mathbf{n}^+ \cdot (\mathbf{x} - \mathbf{x}_\Gamma)). \tag{8}$$

In which $\mathbf{x}$ is the point outside of the crack surface, and $\mathbf{x}_\Gamma$ is any nearest point to point $\mathbf{x}$ on the crack surface; $\mathbf{n}^+$ is a unit normal to the crack surface.

Discretization of level set allows for the evaluation of the level set function at the element level based on the nodal level set values $\varphi_j = \varphi_j(\mathbf{x}_j, t)$ and known classical finite element shape functions $N_j(\mathbf{x})$ [26,35],

$$\varphi(\mathbf{x}, t) = \sum_{j=1}^n N_j(\mathbf{x}, t)\varphi_j. \tag{9}$$

This is practically an important concept for implicitly defining the level set function for describing a general moving interface. This simple procedure of defining the level set function can be widely used in some other method. Another major advantage of this approximation is that the derivatives of the level set function can be obtained by the classical finite element shape functions,

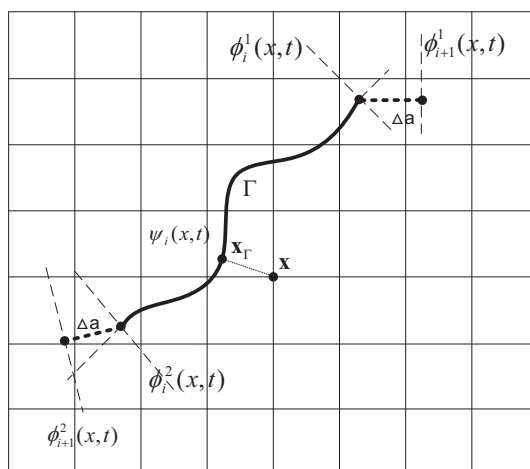$$\varphi_{,i}(\mathbf{x}, t) = \sum_{j=1}^n N_{j,i}(\mathbf{x}, t)\varphi_j. \tag{10}$$

Fig. 4. Level set model.

Based on the above theory, the normal vector $\mathbf{n}$ to the interface Γ at a point $\mathbf{x} \in \Gamma$ can then be defined as

$$\mathbf{n} = \frac{\nabla \varphi(\mathbf{x}, t)}{\|\nabla \varphi(\mathbf{x}, t)\|}. \tag{11}$$

3.2. Tracking crack front

Used the theory of the above section, the crack surface can be decrypted and tracked. But only one level set function of $\varphi(\mathbf{x}, t)$ is not generally sufficient to describe the crack, the same as aforementioned theory, another level set function at the crack tip $\phi^i(\mathbf{x}, t)$ is defined. The crack tip is represented as the intersection of the zero level set function of $\varphi(\mathbf{x}, t)$ with another zero level set function of $\phi^i(\mathbf{x}, t)$, where i is the number of tips on a given crack. So the crack tip level set function $\phi^i(\mathbf{x}, t)$ is generally assumed to be orthogonal to $\varphi(\mathbf{x}, t)$ [26,35], which is shown in Fig. 4,

$$\nabla \varphi(\mathbf{x}, t) \nabla \phi(\mathbf{x}, t) = 0. \tag{12}$$

The same as Eq. (9), the level set function $\phi^i(\mathbf{x}, t)$ can also be interpolated over the mesh by the same finite element shape functions,

$$\phi^i(\mathbf{x}, t) = \sum_{j=1}^{n} N_j(\mathbf{x}) \phi_j^i(\mathbf{x}_j, t). \tag{13}$$

According to the aforementioned theory, the values of level set functions are stored only at nodes, and the values of all other points can be interpolated from their nodes values.

For memory saving, only values of related part of nodes are calculated and stored. Crack growth is modeled by appropriately updating the functions of $\phi^i(\mathbf{x}, t)$ and $\varphi(\mathbf{x}, t)$, and the calculation grid is not changed in all over of the calculation.

4. Discontinuous cellular automaton theory

In the last two sections, the enriched shape functions are obtained, and the crack location and it growth path are tracked by the level set functions. The discretization of the model and discontinuous cellular automaton procedure will be given in this section.

4.1. Discretization and integration

Considering a body Ω, with the boundary Γ, and the strong form of the equilibrium equation can be written as

$$\nabla \cdot \boldsymbol{\sigma} + \mathbf{b} = 0 \quad \text{in} \quad \Omega, \tag{14}$$

$$\boldsymbol{\sigma} \cdot \mathbf{n} = \bar{\mathbf{t}} \quad \text{on} \quad \Gamma_t, \tag{15}$$

$$\mathbf{u} = \bar{\mathbf{u}} \quad \text{on} \quad \Gamma_u, \tag{16}$$

$$\boldsymbol{\sigma} \cdot \mathbf{n} = 0 \quad \text{on} \quad \Gamma_c, \tag{17}$$

where $\mathbf{n}$ is the unit outward normal to Ω, $\bar{\mathbf{u}}$ and $\bar{\mathbf{t}}$ are prescribed displacements and tractions, respectively, and Γ_u, Γ_t and Γ_c are traction, displacement and crack boundaries, respectively, and $\mathbf{b}$ is body force.

Based on Eqs. (14)–(17), one can get the weak form for linear elastostatics, which can be stated as

$$\int_{\Omega} \boldsymbol{\sigma} \cdot \varepsilon d\Omega = \int_{\Omega} \mathbf{b} \cdot \delta \mathbf{u} d\Omega + \int_{\Gamma} \bar{\mathbf{t}} \cdot \delta \mathbf{u} d\Gamma. \tag{18}$$

Discretization of Eq. (18) using the procedure of Eq. (5) results in a discrete system of linear equilibrium equations for each node,

$$\mathbf{K}^e \mathbf{u}^e = \mathbf{f}^e, \tag{19}$$

where $\mathbf{K}^e$ is the nodal stiffness matrix, $\mathbf{u}^e$ is the nodal vector of degrees of nodal freedom for both classical and enriched ones, and $\mathbf{f}^e$ is nodal vector of external force. In this method the assembled matrix and vectors are not needed. And the detail of matrix $\mathbf{K}^e$ and $\mathbf{f}^e$ can be referred to reference [34].

4.2. Discontinuous cellular automaton model (DCA)

The basic procedure of the traditional numerical methods can be summarized as the following steps: discretization of the object, approximation of the shape function, forming the stiffness matrix of node, assembling the overall stiffness of all nodes, solving the overall linear equations. Used discontinuous cellular automaton, the equilibrium state of the object can

be obtained through the self-organization phenomenon formed by the one-another transfer of the information between nodes. Based on this theory, the localization property of object can be easily treated, and the behavior of the cell is thought to be essentially local, in other words, the state of one cell is just determined by the states of itself and its neighbors.

As mentioned, there are three advantages for this theory. One is no need to assemble the overall matrix, especially for the enriched nodes, the degrees for some nodes may be different, which may bring some difficulty for the assembling operation. The second is that it is easily to consider the local properties of the cell, because the updating rule of DCA is only applying on the local cell. The third one is that the large-scale simulation of the failure process can be performed on the mesoscopic scale because of the easy implementation of parallel algorithm.

The DCA model is composed of cell, cell space, cell state, crack, neighborhood and updating rules and so on, and the relation between those components can be seen in Fig. 5. Besides, DCA model includes the continuous cell and discontinuous cell, and in this paper, only the latter is developed, and the former can be seen in [31].

4.2.1. Cell

As the basic component, the cell consists of cell nodes N_i, corresponding cell elements E_i^j and its neighbor cell nodes N_i^k, in which cell nodes include classical finite element nodes, the Heaviside enriched nodes and the exact near-tip asymptotic field functions enriched nodes and cell elements consist of classical finite elements, penetrated elements and crack tip elements [31,36].

4.2.2. Cell space and its states

According to finite element type, 2-D cell space can be rectangular, triangular, hexagon and so on. In order to describe the cell states, a series of physical and mechanical values must be defined to determine its different states. For a DCA model, it is composed of the degree values vector of nodal freedom $\mathbf{u}^h = \{\mathbf{u}, \mathbf{a}, \mathbf{b}\}$, in which $\mathbf{u}$ is traditional degree of nodal freedom, $\mathbf{a}$ is Heaviside enriched degree of nodal freedom and $\mathbf{b}$ is crack tip field function enriched degree of nodal freedom; material property of thickness t, Young's modulus E, Poisson's ratio μ and fracture toughness K_{IC}; cell nodal forces vector $\mathbf{f} = \{\mathbf{f_u}, \mathbf{f_a}, \mathbf{f_b}\}$, in which the subscript $\mathbf{u}$, $\mathbf{a}$ and $\mathbf{b}$ are represented traditional, Heaviside enriched and the exact near-tip asymptotic field functions enriched degrees of nodal freedom respectively; elastic strain ε_e, equivalent plastic strain ε_p and equivalent stress intensity factor K_{Ie} and so on.

4.2.3. Neighborhood

Because only the states of cell itself and its neighbors are taken into account when the updating rules are constructed, neighbor structure is the most essential character of cell space. So the relation between a cell and its neighbors is constructed in this method, which can be seen in Fig. 6.

4.2.4. Continuity to discontinuity model

In DCA model, the discontinuity may exist in some cellular elements, which can be seen in Fig. 6. The location of the crack will determine the cellular node type, cellular element type and cellular automaton model. And in this method, the crack path is tracked by the level set functions. By way of the values of level set functions, the node cellular type, element cellular type and cellular automaton model are updated, especially for some cells, which change from continuous cellular automaton model to discontinuous cellular automaton model.

4.2.5. Updating rules

The updating rules are the most important part of the DCA model, because the updating rules will determine the stress state of a cell element [31,36].
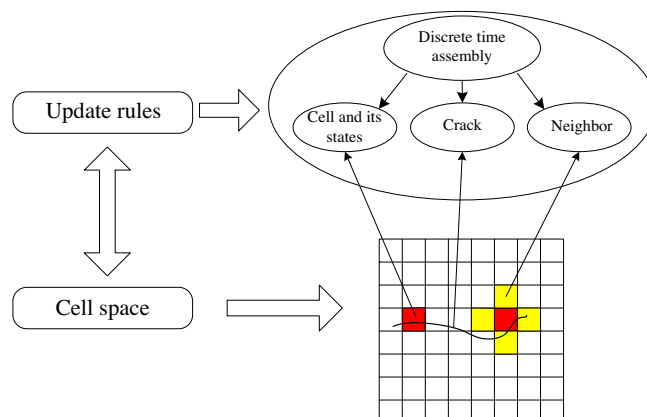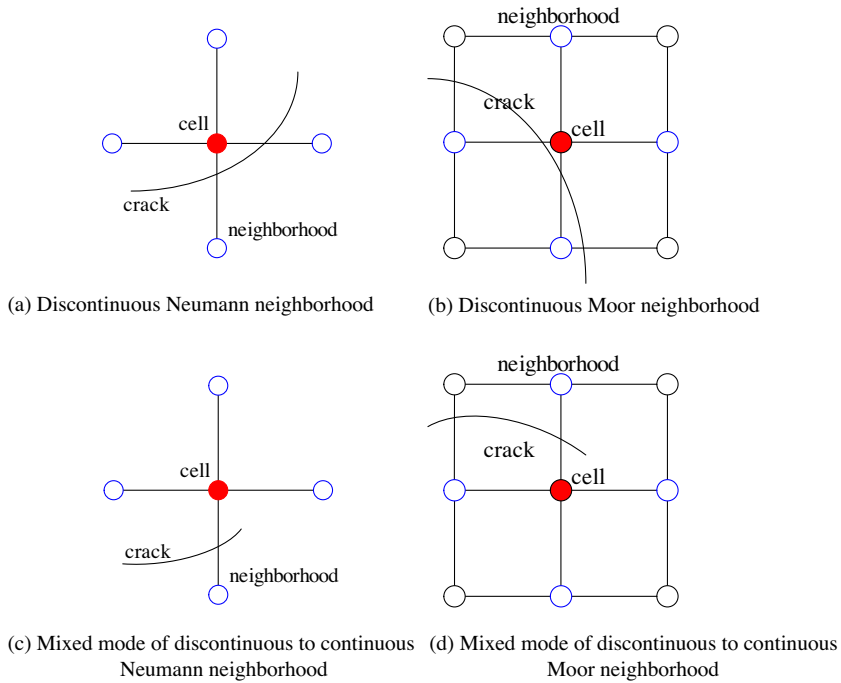

Fig. 5. The relation between the DCA components.

(a) Discontinuous Neumann neighborhood   (b) Discontinuous Moor neighborhood

(c) Mixed mode of discontinuous to continuous   (d) Mixed mode of discontinuous to continuous
    Neumann neighborhood   Moor neighborhood
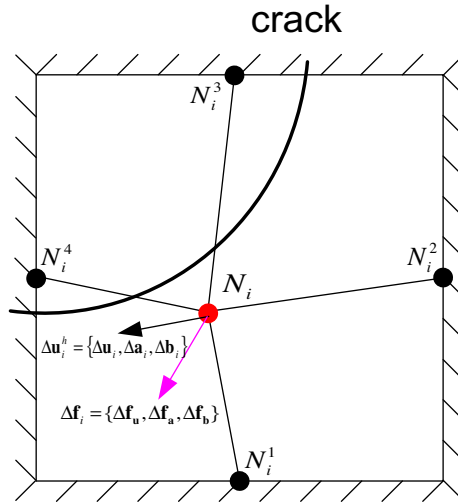
Fig. 6. Cellular neighborhoods.

Fig. 7. Elastic state of cell.

Consider a cellular node N_i for a plane elastic problem, the displacement of this node can be obtained due to the effect of nodal force vector $\mathbf{f}_i = \{\mathbf{f}_i^u, \mathbf{f}_i^a, \mathbf{f}_i^b\}$ and restrict all degrees of the nodal freedom on its neighbor cell nodes N_i^k, which can be shown in Fig. 7. The relation between the incremental force and incremental deformation can be reflected into two steps. Firstly, the nodal force increment $\Delta\mathbf{f}_i = \{\Delta\mathbf{f}_i^u, \Delta\mathbf{f}_i^a, \Delta\mathbf{f}_i^b\}$ will lead the cell node N_i to produce the displacement increment $\Delta\mathbf{u}_i^h = \{\Delta\mathbf{u}_i, \Delta\mathbf{a}_i, \Delta\mathbf{b}_i\}$. Then, the displacement increment $\Delta\mathbf{u}_i^h$ on the cell node N_i will lead its neighboring cell nodes to produce the nodal force increment $\Delta\mathbf{f}_i^k$.

Therefore, the process of the DCA updating rules is: increment of nodal force leads to the increment of nodal displacement, and the increment of nodal displacement leads to the increment of nodal force of its neighboring nodes, until the system static equilibrium is achieved, in other words, the self-organization phenomenon of $\Delta\mathbf{u}_i^h \to 0$ and $\Delta\mathbf{f}_i^k \to 0$ appears. So the updating steps can be given as:

(1) The equilibrium equation of the cell node N_i can be described as

$$\mathbf{K}_i \Delta \mathbf{u}_i^h = \Delta \mathbf{f}_i. \tag{20}$$

In which $\mathbf{K}_i$ is the stiffness of cell node N_i, $\Delta \mathbf{u}_i^h = \{\Delta \mathbf{u}_i, \Delta \mathbf{a}_i, \Delta \mathbf{b}_i\}$, $\Delta \mathbf{f}_i = \{\Delta \mathbf{f}_i^u, \Delta \mathbf{f}_i^a, \Delta \mathbf{f}_i^b\}$ are increment of degrees of nodal freedom and nodal force respectively of cell node N_i.
Calculate the increment of degrees of nodal freedom $\Delta \mathbf{u}_i^h$ via the increment of nodal force $\Delta \mathbf{f}_i$.

(2) Restrict all degrees of nodal freedom on all neighboring cell N_i^k, which can be seen in Fig. 7.
(3) Obtain the nodal force increment $\Delta \mathbf{f}_i^k$ of the neighboring cell N_i^k via $\Delta \mathbf{u}_i^h$ from the following equation

$$\Delta \mathbf{f}_i^k = \mathbf{K}_i^k \Delta \mathbf{u}_i^h, \tag{21}$$

where $\mathbf{K}_i^k$ is the stiffness of neighboring cell N_i^k.

(4) Finish the calculation of steps (1)–(3) on all cell nodes, until $\Delta \mathbf{u}_i^h \to 0$ and $\Delta \mathbf{f}_i^k \to 0$ appear.
(5) Calculate equivalent stress intensity factor K_{Ie}, and judge whether the crack propagation can be occur according to fracture toughness, and finish the crack growth simulation. In order to ensure the accuracy of present method, interaction integral method and equivalent domain integral are combined to use to calculate the stress intensity factor, which are given as,

$$M^{(1,2)} = \int_A \left[\sigma_{ij}^{(1)} \frac{\partial u_j^{(2)}}{\partial x_i} + \sigma_{ij}^{(2)} \frac{\partial u_i^{(1)}}{\partial x_i} - W^{(1,2)} \delta_{1j} \right] \frac{\partial q}{\partial x_j} dA, \tag{22}$$

where $W^{(1,2)} = \sigma_{ij}^{(1)} \varepsilon_{ij}^{(2)} = \sigma_{ij}^{(2)} \varepsilon_{ij}^{(1)}$, and A is the integral domain, which can be seen in Fig. 8; and q is weight function, on nodes which are located inside the circle $q = 1$, on nodes which are located outside the circle $q = 0$, on the other location of the integral element $q = \sum_{i=1}^{4} N_i q_i$, the superscript 1 is the actual stress state, and the superscript 2 is an auxiliary stress state. $M^{(1,2)}$ can also given as

$$M^{(1,2)} = \frac{2}{E^*} \left(K_I^{(1)} K_I^{(2)} + K_{II}^{(1)} K_{II}^{(2)} \right), \tag{23}$$

where $E^* = E$ for plane stress problem and $E^* = E/(1 - v^2)$ for plane strain problem. If give $\sigma_{ij}^{(2)}$ and $u_i^{(2)}$ as the pure opening mode I crack tip filed, $K_{II}^{(2)} = 0$, then the stress intensity factor K_I of actual stress state 1 can be solved, and the same work can be applied for K_{II}.

For mixed mode crack propagation, many criteria can be used, we take maximum circumferential tensile stress as example, in this case,

$$\frac{K_I}{K_{IC}} \cos^3 \frac{\theta}{2} - \frac{3K_{II}}{2K_{IC}} \cos \frac{\theta}{2} \sin \theta = 1, \tag{24}$$

or

$$K_{eq} = K_I \cos^3 \frac{\theta}{2} - \frac{3}{2} K_{II} \cos \frac{\theta}{2} \sin \theta. \tag{25}$$
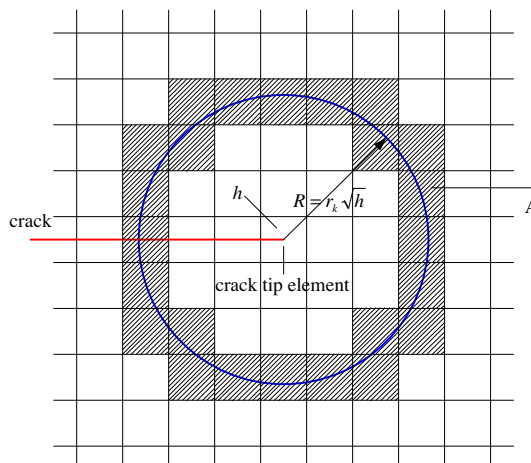

Fig. 8. Integration domain.

(6) According to the crack growth information of step (5), update level set functions $\varphi(\mathbf{x}, t)$ and $\phi^i(\mathbf{x}, t)$, and update node type and element type for all nodes and elements and so on. The updating steps are given as

Step 1: Determine $\phi^{k,r}$, $\phi^{k,r} = (x - x_k)\frac{\mathbf{v}_x}{\|\mathbf{v}\|} + (y - y_k)\frac{\mathbf{v}_y}{\|\mathbf{v}\|}$, in which $\mathbf{v} = (\mathbf{v}_x, \mathbf{v}_y)$ is prescribed velocity vector.

Step 2: Determine φ_{n+1}, $\varphi_{n+1} = \pm\left|(x - x_k)\frac{\mathbf{v}_y}{\|\mathbf{v}\|} + (y - y_k)\frac{\mathbf{v}_x}{\|\mathbf{v}\|}\right|$.

Step 3: The updated crack tip is given as $\phi_{n+1}^k = \phi^{k,r} - \Delta t\|\mathbf{v}\|$, and $\phi(x, t) = \max_k(\phi^k)$ for k crack tips.

(7) Check cellular automaton model, especially for cells which change from continuous model to discontinuous model, and update corresponding model data.

4.2.6. convergence study for DCA

According to the theory of updating rule of cellular automaton and numerical analysis, the present method is equal to the relaxation method for linear system, and at this time, the necessary and sufficient condition is

$$\rho(\mathbf{A}) < 1.0. \tag{26}$$

In which A is stiffness matrix of the present method, and $\rho(\mathbf{A})$ is spectral radius.

For stiffness matrix of the present method, according to the theory of finite element method and extended finite element method, the stiffness matrix of the present method is symmetrical, positive, and diagonally dominant. And according to numerical analysis theory, if matrix A is symmetrical, positive, and diagonally dominant, then $\rho(\mathbf{A}) < 1.0$ is satisfied at all time, so the updating step of the present method converges at all conditions.

5. Numerical simulation

In this method, equivalent domain integral method and interaction integral method are combined to calculate the stress intensity factor, in which the mechanical properties on integral point are all easily to obtain, and the integral element is coincide to the finite element, so that it is easily to deal. Besides, the maximum circumferential tensile stress criterion is used to judge the crack growth.

5.1. Interactive crack growth of double internal cracks

5.1.1. Path of crack growth

The interaction of crack growth will occur when the crack tips closely approach with each other [37]. The computation model about the interaction of double internal cracks is shown in Fig. 9 [37]. The non-dimensional size of calculation model is given as, $c/a = 1.0, d/a = 1.0$ and $a/B = 0.15$. The Young's modulus and the Poisson's ratio are assumed to be 200 GPa and 0.3, respectively. The uniform tensile stress, σ_0, is applied at the upper and bottom edges of the plate. a_{eq} represents the equivalent half crack length, which is the half length between tip 1 and tip 4.
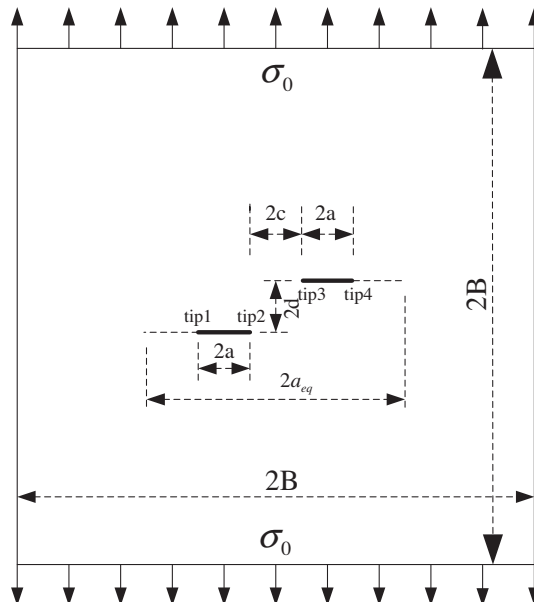

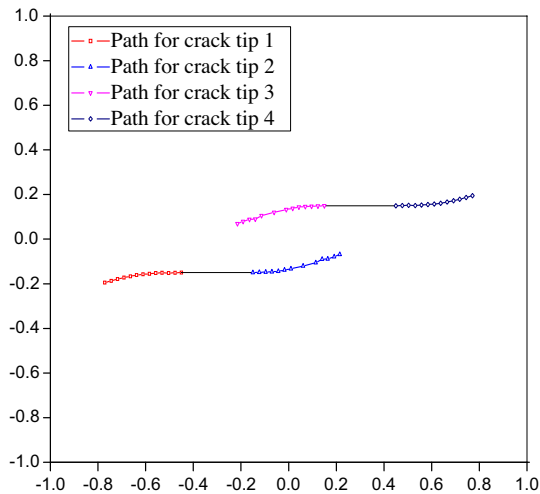Fig. 9. Model of double internal cracks.

Fig. 10. Predicted crack growth paths of double internal cracks.

The simulated growth paths of the four crack tips are plotted in Fig. 10, in which both the interior crack tips (Tip 2 and Tip 3) and exterior crack tips (Tip 1 and Tip 4) are almost straight in the beginning of their growing, then the interior crack tips come closer to each other, and tend to coalesce. While the exterior crack tips extend in the opposite direction of their corresponding interior ones. And the present method results are consistent with those of the Ref. [37].

The non-dimensional stress intensity factors (SIF) of those crack tips are shown in Fig. 11, in which $K_{IO} = \sigma_0\sqrt{\pi a_{eq}}$. It can be seen in this figure that the stress intensity factors of exterior crack tips increase with their growing, and they approach to the solution of a central crack plate with uniform tension, when the exterior crack tips extend close to the edge of the plate. But the stress intensity factors of the interior crack tips increase in the beginning, then decrease when they extend to the upper or the bottom of another crack, which are agreed with the results of reference [37].

5.1.2. Comparison of computer memory and time between XFEM and DCA

It is known that the calculation of the present method is located on the local of the element and no assembled global stiffness matrix is needed. So it has an advantage of computer memory saving. Fig. 12 plots the computer memory comparison between DCA, XFEM with and without half-bandwidth storage technique. It can be seen that much less computer memory is needed in DCA than that of XFEM with and without half-bandwidth storage technique, and which is much more obvious when the element number is much larger, the reason for which is that the calculations is only located on each node, and no assembled matrix is needed in the whole calculation, but for XFEM, a total assembled matrix is inevitable, so the computer memory expanse is much larger for XFEM.

5.1.3. Comparison of computer time between XFEM and DCA

In order to compare the calculation efficiency of DCA and XFEM, the CPU time for different number of element between the present method and XFEM are plotted in Fig. 13. it can be seen that the computer time of the present method is a little larger than that of XFEM, because that cellular automaton updating is time-consuming, which will be studied in next work for parallel version of DCA to improve the calculation efficiency. The calculation computer system is given as: CPU: Intel Core 2 Duo E8400 @ 3.0 GHz, Memory: 4 GB, operating system: Windows xp.

5.1.4. Convergence of the present method

In order to verify the effectiveness of the present method, the convergence of the present method is studied, which can be seen in Fig. 14, it is shown that the present method can smoothly converge to the exact values, although many steps are needed, because it calculation is only located on the node, each steps can be finished very quickly, and its computer time expense is not very large. Besides, a large number of examples are studied to show that the present method can always converge to the exact value.

5.2. Interactive crack growth of double edge cracks

Melin's researches are shown that originally collinear edge cracks under predominantly Mode I loading, do not follow a straight crack path, and they seem to avoid each other before coalescence [37,38]). So in this section, a square plate with double edge cracks located at opposite edge of plate is studied. The analysis model is given in Fig. 15. The non-dimensional
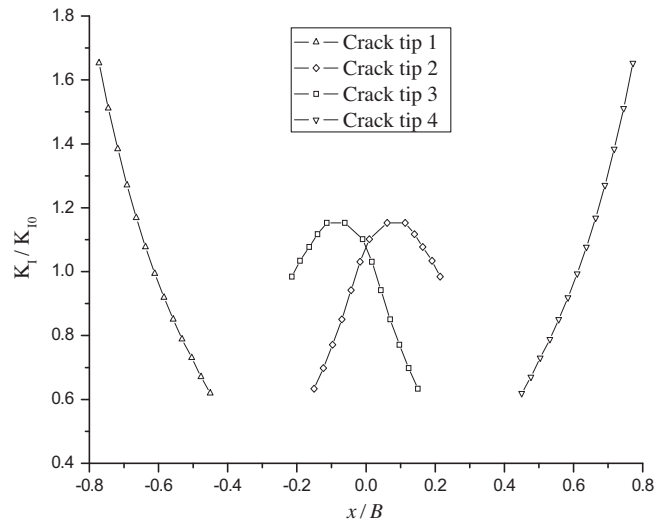
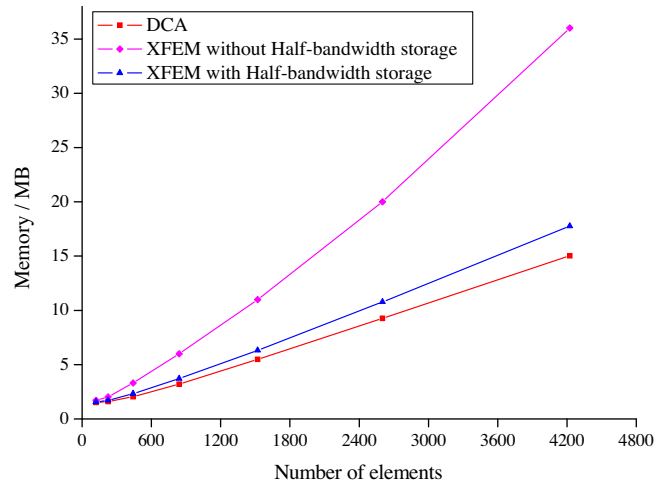**Fig. 11.** Non-dimensional stress intensity factors at four crack tips.

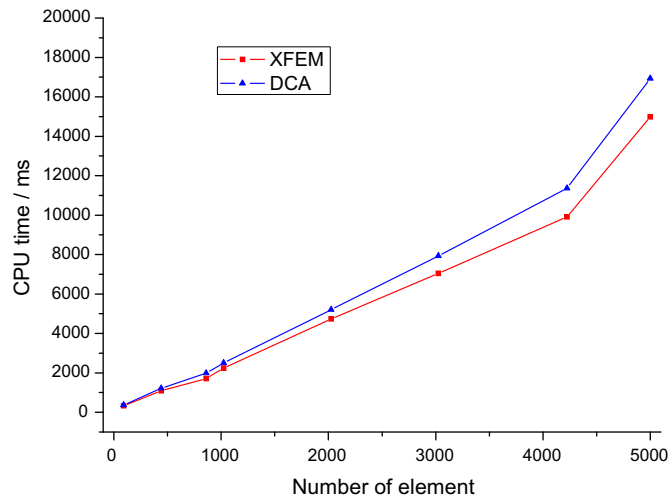**Fig. 12.** Computer Memory comparison between DCA and some other methods.

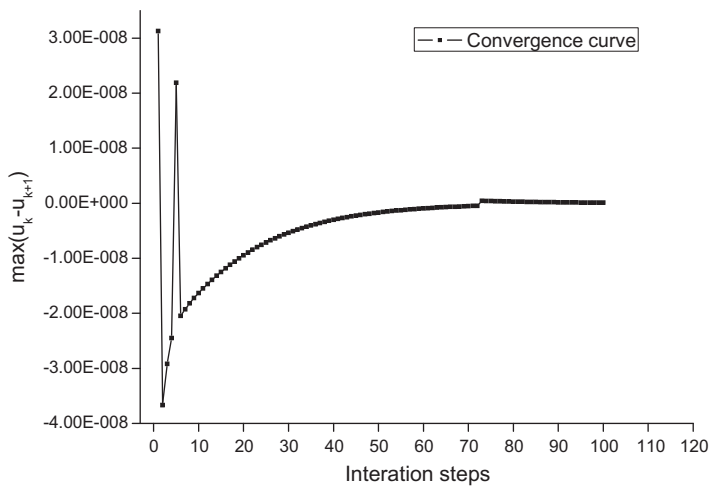**Fig. 13.** Comparison for CPU time between DCA and XFEM with half-bandwidth storage technique.
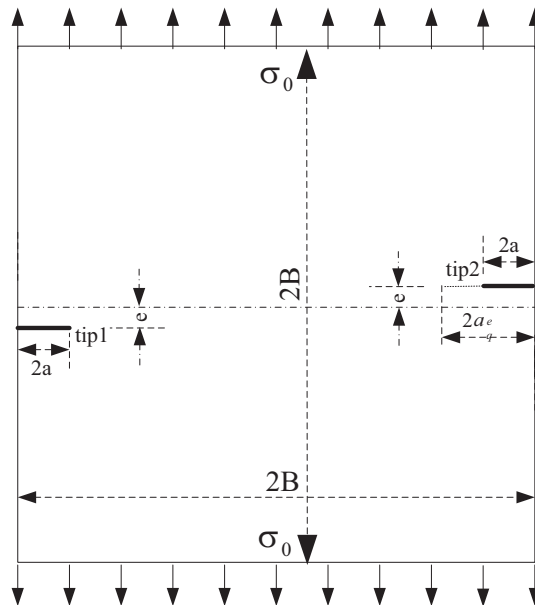
Fig. 14. Convergence of the present method.

Fig. 15. Model of double edge cracks.

geometry of model is assumed to be $a/B = 0.4$ and $e/B = 0.05$. It is shown in Fig. 15 that the initial cracked lines are slightly misaligned. The other parameters are the same as Section 5.1.

Fig. 16(a) shows the simulated paths of double edge cracks by DCA, and Fig. 16(b) plots the predicted crack growth paths of double edge cracks by XFEM, which are calculated by the codes by the author. It is shown in these two figures that the present method results are almost the same as the results by XFEM. According those two figures, we can see: different to double internal cracks, two crack tips in this example seem to avoid each other in the beginning of their growth. In the beginning, the crack tips slightly rotate to the clockwise direction, because the material between the two crack tips is compressed in the initial crack direction, and after they propagate for a certain distance, they begin to extend in the anti-clockwise direction, and tend to coalesce.

The same as the results of double internal cracks, the stress intensity factors of those crack tips increase in the beginning of their propagation, and approach a certain distance, they decrease, which can be seen in Fig. 17. One can see that a great agreement can be obtained between the results of the present method and those of Ref. [39].
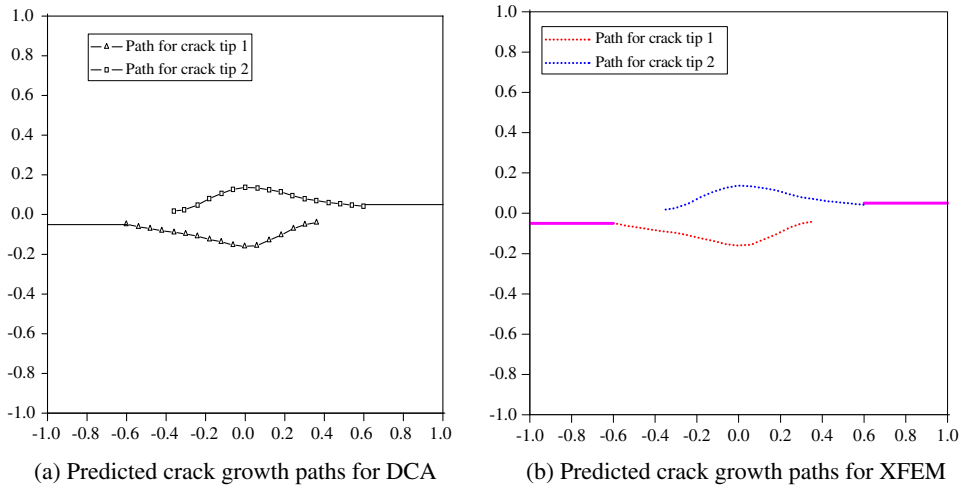
(a) Predicted crack growth paths for DCA   (b) Predicted crack growth paths for XFEM

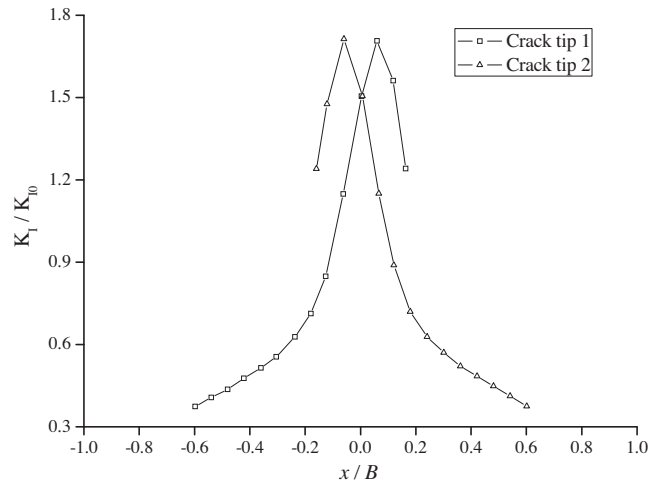**Fig. 16.** Comparison for predicted crack growth paths of double edge cracks between DCA and XFEM.

Fig. 17. Non-dimensional stress intensity factors at two crack tips.

5.3. Shielding effect of multiple cracks

Some researches are shown that interaction and shielding effect occur when multiple cracks are located closely in a small zone. The stress intensity factors of each crack tip are quite different, because the geometries of cracks are different with each other, so the growth paths of cracks vary with each other. In this section three cracks with different length in a square plate are considered to illustrate the shielding effect of multiple cracks.

A non-dimensional geometry model of multiple cracks is shown in Fig. 18, which bears a uniform tension σ_0 on the upper and bottom edge, and the coordinates and the distances among each crack are shown in this figure. In order to study the shielding effect of multiple cracks, only the interior crack tips are considered in this example.

The simulated paths of each interior crack tip are shown in Fig. 19. Because the different lengths of each crack, the stress intensity factors vary widely, so the growth velocities are also different, the growth velocity of crack tip 2 is very small, especially when the long crack propagates through it. In other word, the growth of the long crack brings a shielding effect to the short one. On the contrary, a largely deflection of the path of long crack is occurred because of the influence of the short cracks.

The non-dimensional stress intensity factors of crack tip 1 are shown in Fig. 20, in which $K_{IO} = \sigma_0\sqrt{\pi a_{eq}}$ and a_{eq} is the real crack length of the long crack. It can be seen that the stress intensity factor of crack tip 1 increases in the beginning, and attaches maximum when it meets the crack tip 2, and then it decreases. When it propagates to the below of crack 2, the stress intensity factor reaches minimum, and then it increases again. And the same effect can be seen when crack tip 1 passes
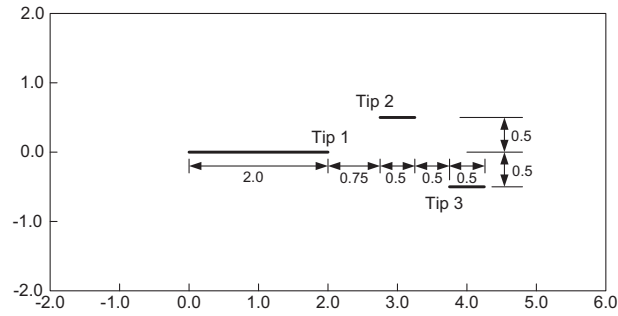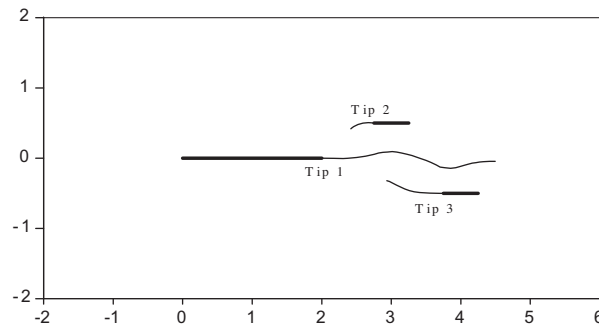
Fig. 18. Model of multiple cracks.

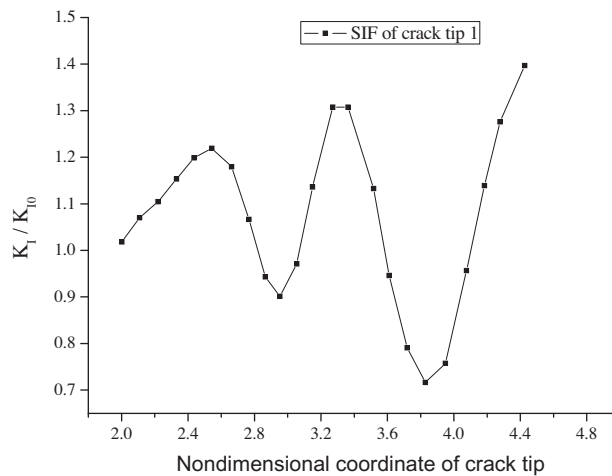**Fig. 19.** Predicted crack growth paths of multiple cracks.

Fig. 20. Stress intensity factor of crack tip 1.

though crack 3. The results are shown that the stress intensity factors and growth paths are affected by each other when multiple cracks are considered.

6. Conclusions

A numerical method of discontinuous cellular automation method has been proposed for the problems of multiple cracks growth in this paper, in which the level set method, the discontinuous enriched shape functions and discontinuous cellular automaton theory are combined. Therefore, the present method has the following advantages,

(1) No remeshing is needed in calculation the crack growth, because of the usage of level set method and discontinuous enriched shape functions.
(2) No assembled stiffness matrix is needed, but only the nodal stiffness matrix is needed in the whole calculation, owing to the application of discontinuous cellular automaton.
(3) High accuracy and efficiency can be easily achieved as a result of the combination of discontinuous cellular automaton and discontinuous enriched shape functions.
(4) Less computer memory requirement than that of XFEM is achieved.
(5) The numerical examples of multiple cracks growth have been given to shown that the present method is accurate and efficient. Because discontinuous cellular automaton has the intrinsic properties of time evolution, locality and parallelization, it can be easily extended to heterogeneous and large-scale problems, so its parallel version will be further studied for large-scale practical engineering simulation.

Acknowledgments

References

[1] R. Barsoum, Triangular quarter-point elements as eleatic and perdectly-plastic crack tip elements, Int. J. Numer. Methods Eng. 11 (1977) 85–98.
[2] E.F. Rybicki, M.F. Kanninen, A finite element calculation of stress intensity factors by a modified crack closure integral, Eng. Fract. Mech. 9 (1977) 931–938.
[3] G.E. Blandford, A.R. Ingraffea, J.A. Liggett, Two-dimensional stess intensity factor computations using boundary element method, Int. J. Numer. Methods Eng. 17 (1981) 387–404.
[4] Y. Mi, M.H. Aliabadi, Dual boundary element method for three-dimensional fracture mechanics analysis, Eng. Anal. Boundary Elem. 10 (1992) 161–171.
[5] G. Karami, R.T. Fenner, Analysis of mixed mode fracture and crack closure using the boundary integral equation method, Int. J. Fract. 30 (1986) 13–29.
[6] Y.K. Cheung, C.W. Woo, Y.H. Wang, The stress intensity factor for a double edge cracked plate by boundary collocation method, Int. J. Fract. 37 (1988) 217–231.
[7] Y.H. Wang, Y.L. Wu, F. Yu, Fracture calculation of bending plates by boundary collocation method, Appl. Math. Mech. Engl. 24 (2003) 684–690.
[8] Y.Y. Lu, T. Belytschko, L. Gu, A new implementation of the element free Galerkin method, Comput. Methods Appl. Mech. Eng. 113 (1994) 397–414.
[9] M. Fleming, Y.A. Chu, B. Moram, T. Belytschko, Enriched element-free Galerkin methods for crack-tip fields, Int. J. Numer. Methods Eng. 40 (1997) 1483–1504.
[10] P. Krysl, T. Belytschko, The element free Galerkin method for dynamic propagation of arbitrary 3-D cracks, Int. J. Numer. Methods Eng. 44 (1999) 767–800.
[11] S.N. Atluri, T. Zhu, A new meshless local Petrov–Galerkin approach in computational mechanics, Comput. Mech. 22 (1998) 117–127.
[12] S.N. Atluri, J. Sladek, V. Sladek, T. Zhu, The local boundary integral equation and it's meshless implementation for linear elasticity, Comput. Mech. 25 (2000) 180–198.
[13] R.J. Tasy, Y.J. Chiou, W.L. Chuang, Crack growth prediation by manifold method, J. Eng. Mech. 125 (1999) 884–890.
[14] J.M. Melenk, I. Babuska, The partition of unity finite element method: basic theory and applications, Seminar fur Angewandte Mathematik, Eidgenossische Technische Hochschule, Research report No. 96–01, January, CH-8092 Zurich, Switzerland, 1996.
[15] T. Belytschko, T. Black, Elastic crack growth in finite elements with minimal remeshing, Int. J. Numer. Methods Eng. 45 (1999) 601–620.
[16] N. Moes, J. Dolbow, T. Belytschko, A finite element method for crack growth without remeshing, Int. J. Numer. Methods Eng. 46 (1999) 131–150.
[17] C. Daux, N. Moes, J. Dolnow, M. Sukumark, T. Belytschko, Arbitrary branched and intersecting cracks with the extended finite element method, Int. J. Numer. Methods Eng. 48 (2000) 1741–1760.
[18] N. Sukumar, N. Moes, B. Moran, T. Belytschko, Extended finite element method for three-dimensional crack modeling, Int. J. Numer. Methods Eng. 48 (2000) 1549–1570.
[19] J. Dolbow, N. Moes, T. Belytschko, An extended finite element method for modeling crack growth with frictional contact, Comput. Methods Appl. Mech. Eng. 190 (2001) 6825–6846.
[20] Q.Z. Xiao, B.L. Karihaloo, Improving the accuracy of XFEM crack tip fields using higher order quadrature and statically admissible stress recovery, Int. J. Numer. Methods Eng. 66 (2006) 1378–1410.
[21] C.A. Duarte, O.N. Hamzeh, T.J. Liszka, W.W. Tworzydlo, A generalized finite element method for simulation of three dimensional dynamic crack propagation, Comput. Methods Appl. Mech. Eng. 190 (2001) 2227–2262.
[22] T. Strouboulis, I. Babuska, K. Copps, The design and analysis of the generalized finite element method, Comput. Methods Appl. Mech. Eng. 181 (2000) 43–69.
[23] T. Strouboulis, K. Copps, I. Babuska, The generalized finite element method, Comput. Methods Appl. Mech. Eng. 190 (2001) 4081–4193.
[24] S. Osher, J.A. Sethian, Fronts propagating with curvature-dependent speed: algorithms based on Hamilton–Jacobi formulations, J. Comput. Phys. 79 (1988) 12–49.
[25] T. Belytschko, N. Moes, S. Usui, C. Parimik, Arbitrary discontinuities in finite elements, Int. J. Numer. Methods Eng. 50 (2001) 993–1013.
[26] M. Stolarska, D.L. Chopp, N. Moes, T. Belytschko, Modelling crack growth by level sets in the extended finite element method, Int. J. Numer. Methods Eng. 51 (2001) 943–960.
[27] C. Shen, S. Dai, J. Yang, X. Tang, Cellular automata for analysis of plane problem in theory of elasticity, J. Tsinghua Univ. (Sci. & Tech.) 41 (2001) 35–38 [in Chinese].
[28] Z. Gurdal, T. Tatting, Cellular automata for design of truss structures with linear and non-linear response, In: Proceedings of 41st AIAA/ASME/ASCE/AHS/ASC structural dynamics and materials conference, Atlanta, GA, 2000.
[29] R.K. Hopman, M.J. Leamy, Triangular cellular automata for computing two-dimensional elastodynamic response on arbitrary domain, J. Appl. Mech. T ASME 78 (2011) 021020.
[30] M.J. Leamy, Application of cellular automata modeling to seismic elastodynamics, Int. J. Solids Struct. 45 (2008) 4835–4849.
[31] X.T. Feng, P.Z. Pan, H. Zhou, Simulation of the crack microfracturing process under uniaxial compression using an elasto-plastic cellular automaton, Int. J. Rock Mech. Min. Sci. 43 (2006) 1091–1108.
[32] A. Anandarajah, Discrete element method for simulating behavior of cohesive soil, J. Geotech. Eng. ASCE 120 (1994) 1593–1613.

[33] G.H. Shi, Discontinuous Deformation Analysis: A New Numerical Model for the Statics and Dynamics of Deformation Block Structures, PhD Thesis. Berkeley, University of California, 1988.

[34] S. Mohammadi, Extended Finite Element Method for Fracture Analysis of Structures, Blackwell Publishing Ltd, UK, 2008.

[35] J. Sethian, Evolution, implementation and application of level set and fast marching methods for advancing fronts, J. Comput. Phys. 169 (2001) 503–555.

[36] P.Z. Pan, X.T. Feng, J.A. Houdson, Study of failure and scale effects in rocks under uniaxial compression using 3D cellular automata, Int. J. Rock Mech. Min. Sci. 46 (2009) 674–685.

[37] Y. Sumi, Z.N. Wang, A finite-element simulation method for a system of growing cracks in a heterogeneous material, Mach. Mater. 28 (1998) 197–206.

[38] S. Melin, Why do cracks avoid with each other, Int. J. Fract. 23 (1983) 37–45.

[39] Z.L. Li, C. Wang, Advanced Boundary Element Method, Science Press, Beijing, 2008 [In Chinese].